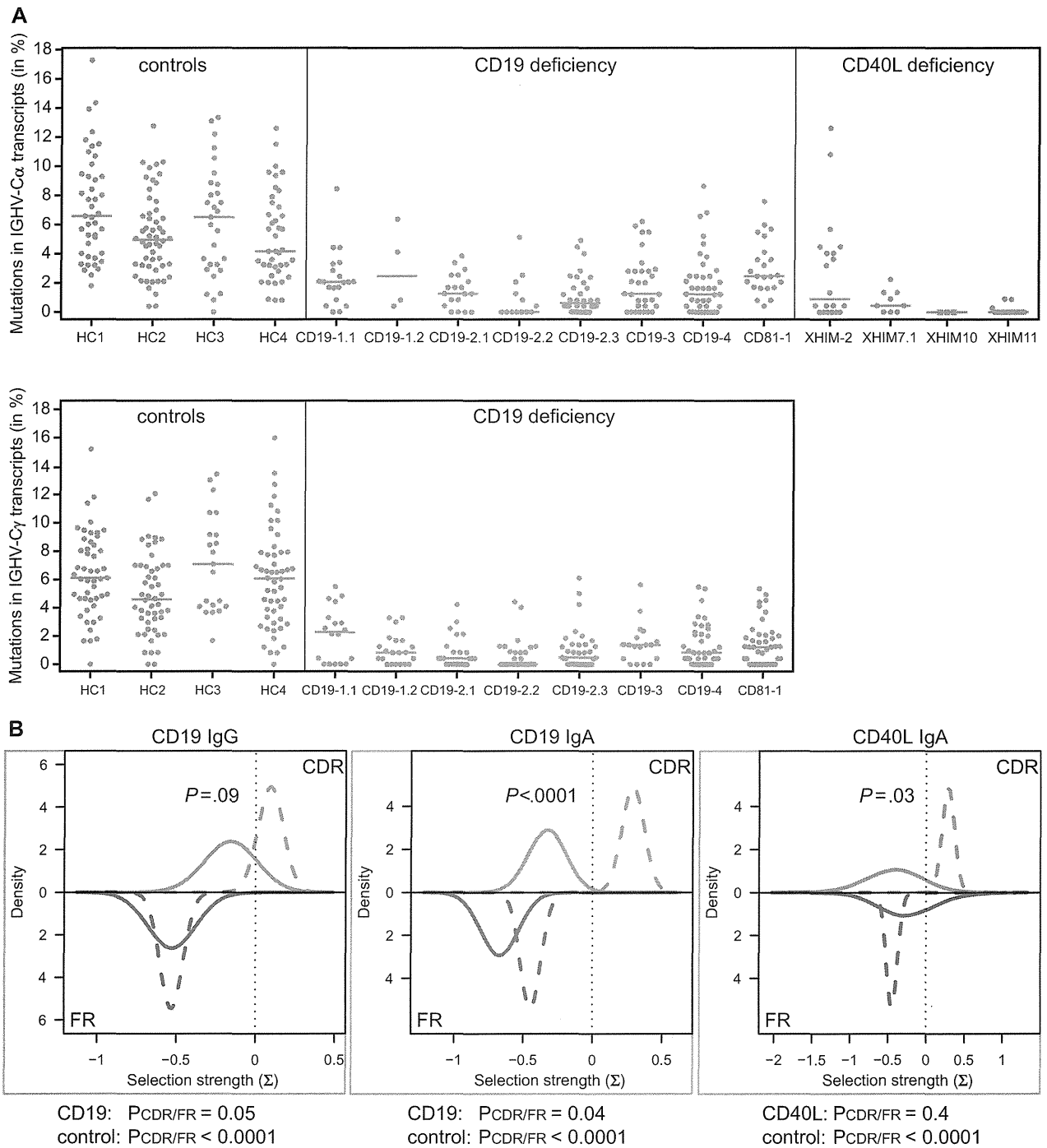

FIG 1. SHM analysis. **A,** Mutation frequencies in *IGHV* genes of Cα and Cγ transcripts of healthy controls (HC) and patients. *Gray dots* represent unique sequences; *red lines* represent median values. Ages: HC1 and HC2, 7 years; HC3 and HC4, 22 years. **B,** Selection for replacement mutations in IGHV-CDRs *(red lines)* and IGHV-FRs *(blue lines)* as determined with the Bayesian estimation of Antigen-driven SELectIoN program.[16] *Solid lines* represent patients; *dotted lines* represent healthy controls. A selection strength of more than 0 is indicative of positive selection.

www.jacionline.org).[9] CD19-deficient patients also showed a marked reduction in all memory B cells, except for the $CD27^{-}IgA^{+}$ subset (Fig E1, *B*). Their natural effector B-cell numbers were more severely decreased than in CD40L-deficient patients, whereas low numbers of circulating $CD27^{-}IgG^{+}$ and $CD27^{+}IgA^{+}$ memory B cells were detectable (Fig E1).

SHM frequencies and patterns

IgA and IgG transcripts using the large IGHV3 and IGHV4 subgroups[27,28] were amplified to study molecular signs of antibody selection. IgG transcripts could not be detected in CD40L-deficient patients. SHM levels in *IGHV* genes of IgA and IgG transcripts were similar between childhood and adult

TABLE I. Targeting and selection of individual mutations in rearranged *IGHV*

	IgA			IgG	
	Control (n = 153)	CD19-deficient (n = 202)	CD40L-deficient (n = 50)	Control (n = 163)	CD19 (n = 221)
Transitions (%)	1394/2725 (51.2)	672/1532 (43.9)*	103/177 (58.2)†	1516/2990 (50.7)	641/1493 (42.9)*
Transversions (%)	1331/2725 (48.8)	860/1532 (56.1)*	74/177 (41.8)†	1474/2990 (49.3)	852/1493 (57.1)*
Transitions at C·G (%)	809/1612 (50.2)	459/1005 (45.7)*	66/99 (66.7)*†	897/1790 (50.1)	384/938 (40.9)*
Targeting of C·G (%)	1612/2725 (59.2)	1005/1532 (65.6)*	99/177 (55.9)†	1790/2990 (59.9)	938/1493 (62.8)
RGYW (%)	644.8/2725 (23.7)	284.3/1532 (18.6)*	40.6/177 (22.9)	745.6/2990 (24.9)	256.5/1493 (17.2)*
WRCY (%)	393.7/2725 (14.4)	287.1/1532 (18.7)*‡	24.6/177 (13.9)	436.4/2990 (14.6)	235.0/1493 (15.7)
WA (%)	309.9/2725 (11.4)	116.5/1532 (7.6)*	21.6/177 (12.2)†	337.8/2990 (11.3)	104.5/1493 (7.0)*
TW (%)	197.6/2725 (7.3)	78.9/1532 (5.2)*	18/177 (10.2)†	183.3/2990 (6.1)	76.9/1493 (5.2)
FR (R/S)	1203/631 (1.9)	817/330 (2.5)*	78/49 (1.6)†	1334/743 (1.8)	822/360 (2.3)*
CDR (R/S)	693/173 (4.0)	274/80 (3.4)	39/11 (3.5)	713/179 (4.0)	235/52 (4.5)

The number of analyzed sequences is indicated in parentheses next to the population name.
All analyses were performed with the JoinSolver program, and the differences between controls and patients were analyzed with the χ^2 test. *R/S*, Ratio between replacement (R) and silent mutations (S).
*Significant differences ($P < .05$) between patient and control cells.
†Significant differences ($P < .05$) between IgA of CD40L and CD19 deficiency.
‡Significant differences ($P < .05$) between IgA and IgG of CD19 deficiency.

controls (median, 4%-7%; Fig 1, *A*). SHM frequencies in CD19-deficient patients were reduced to less than 3% and in CD40L-deficient patients to less than 1%.

CD19-deficient and CD40L-deficient patients showed an accumulation of replacement mutations in CDR1 and CDR2 of rearranged *IGHV* genes, similar to controls (see Fig E2 in this article's Online Repository at www.jacionline.org). Furthermore, IGHV-CDR R/S ratios of controls, CD19-deficient patients, and CD40L-deficient patients were similarly increased as compared to IGHV-FRs and ranged between 3.4 and 4.5 (Table I). However, the increased R/S ratios in CDRs versus FRs do not necessarily reflect selection processes because CDR codons are more susceptible than FR codons to replacement mutations.[29] Therefore, we analyzed the *IGH* sequences with the Bayesian estimation of Antigen-driven SELectIoN program, which determines whether the mutation patterns differed from what can be expected from random targeting.[26] Similar to previous observations,[30] we found positive selection for replacement mutations in the CDR and negative selection in the FR of IgA and IgG transcripts of healthy controls (Fig 1, *B*; dotted lines). In contrast, CD19-deficient and CD40L-deficient patients lacked positive selection of replacement mutations in the CDR. Thus, IgH-switched transcripts in CD19-deficient and CD40L-deficient patients showed impaired SHM levels with reduced selection for replacement mutations in the CDR.

Impaired immunoglobulin class switching to downstream constant regions

The human *IGH* locus contains 2 IgA and 4 IgG constant regions (Fig 2, *A*). IgA2 was almost as frequently used as IgA1 in healthy controls. This was significantly reduced in CD19-deficient (23%) and CD40L-deficient patients (4%; Fig 2, *B*). Furthermore, the SHM frequencies did not differ between IgA1 and IgA2 transcripts and were strongly reduced for both isotypes in CD19-deficient and CD40L-deficient patients (Fig 2, *C*).

The IgG subclass distribution in CD19-deficient patients was also skewed toward the usage of IgM-proximal IgG subclasses (Fig 2, *B*). While in controls, IgG1 (56%) and IgG2 (35%) were mostly used, CD19-deficient patients mostly used IgG1 (73%) and IgG3 (12%). The SHM frequencies in all subclasses were significantly lowered in CD19-deficient patients than in controls, but these increased with more downstream IgG subclass usage (Fig 2, *C*). A similar trend was seen for controls, but this was not significant. We therefore conclude that the IgG subclass distribution molecularly reflects the defective secondary immune responses of CD19-deficient patients.[17]

Immunoglobulin repertoire selection for superantigen binding

Similar to healthy controls, CD19-deficient and CD40L-deficient patients showed diverse use of *IGHV3* subgroup genes with *IGHV3-23*, *IGHV3-30*, and *IGHV3-48* predominating (not shown). The *Staphylococcus aureus* virulence factor protein A (SpA) triggers supraclonal B-cell responses through interactions with several contact residues in the FR1 and FR3 of *IGHV3*-encoded BCRs.[31] To study the selection for SpA binding, we analyzed the frequencies of IgG and IgA rearrangements with mutations in 1 or more of the 7 critical residues: ARG/LYS-20, GLY-74, ARG-75, THR-77, SER-79, GLN-90, and ASN-92 (Fig 3, *A*).[31] The mutation frequencies in *IGHV3* transcripts from controls and CD19-deficient patients were compared with *IGHV1/4* transcripts that cannot bind SpA. The number of transcripts of CD40L-deficient patients was too low for this analysis. The frequencies of mutated *IGHV1/4* genes were similar to the theoretical chance, that is, 7 times the overall replacement mutation frequency (Fig 3, *B*). These mutation rates were much higher in controls (63% and 76%) than in CD19-deficient patients (28% and 24%), due to the lower replacement mutation rates in the patients. Importantly, in both controls and CD19-deficient patients, the frequencies of *IGHV3* rearrangements with mutated core residues were significantly lower than those of *IGHV1/4* rearrangements, despite comparable overall mutation frequencies. Thus, *IGHV3* rearrangements are selected for maintaining SpA superantigen binding, a process that is not dependent on CD19.

Because SpA superantigen binding was normally retained in CD19-deficient patients, whereas other immunoglobulin selection processes were abnormal, we addressed whether SpA is able to activate CD19-deficient B cells. In line with previous observations, CD19-deficient patients showed impaired Ca^{2+} influx following anti-IgM stimulation (Fig 3, *C*).[17-19] In contrast, *S aureus* Cowan I lysate, in which SpA is the dominant B-cell

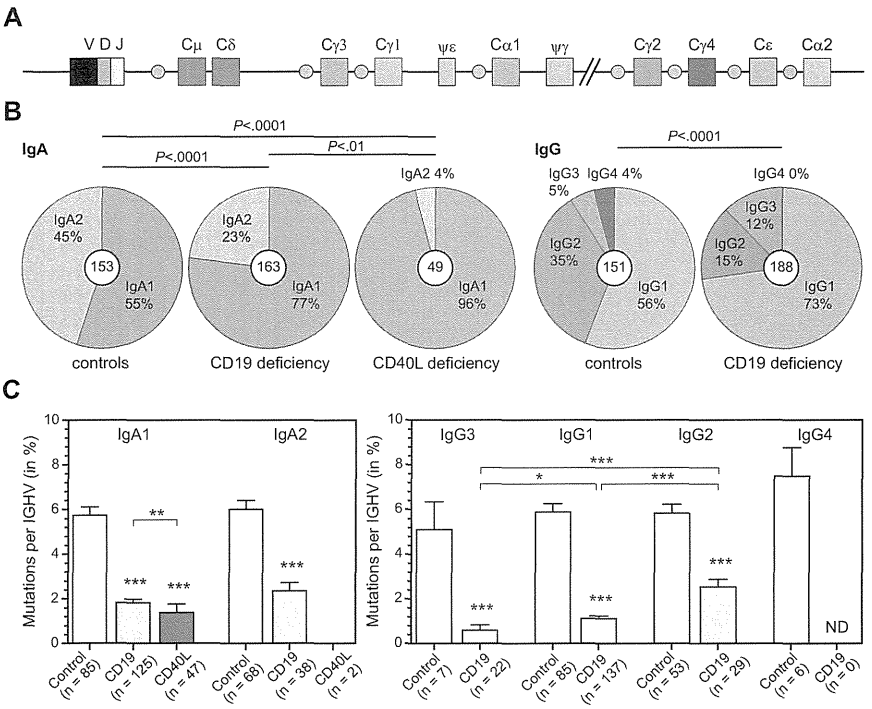

FIG 2. IgA and IgG subclass analysis. **A,** Schematic representation of the constant region of the human *IGH* locus. **B,** Distribution of IgA and IgG subclass use in switched transcripts of healthy controls, CD19-deficient patients, and CD40L-deficient patients. Total numbers of analyzed sequences are indicated in the center of each plot. Differences in the distributions were statistically analyzed with the χ^2 test. **C,** *IGHV* mutation frequencies in distinct IgA and IgG subclasses (mean ± SEM). *ND,* Not detected. Statistical significance was calculated with the Mann-Whitney test. $*P < .05$; $**P < .01$; and $***P < .001$.

stimulant,[32] induced a normal initial Ca^{2+} influx followed by an increased baseline level that is reminiscent of BCR signaling.[33] Thus, CD19-deficient B cells display normal signaling and immunoglobulin selection for SpA superantigen binding.

Immunoglobulin repertoire selection against inherently autoreactive properties

Within the *IGHV4* subgroup, the *IGHV4-34* and *IGHV4-59* genes were most frequently used in naive mature B cells of healthy controls, likely because of their highly efficient recombination signal sequences.[34,35] *IGHV4-34* genes were hardly used in IgA and IgG transcripts of controls (Fig 4, *A* and *B*) because they display inherent autoreactivity in their FR1 that binds the I antigen on red blood cells.[36] Moreover, 3 of 5 *IGHV4-34* transcripts in control IgG and IgA transcripts were mutated in 1 or more of the I antigen–binding residues—TRP-7, ALA-23, TYR-25[36]—thus likely removing autoreactivity. The selection against *IGHV4-34* use was impaired in CD19-deficient and CD40L-deficient patients (Fig 4, *A* and *B*). Furthermore, nearly all these transcripts (24 of 25 of CD19 and 2 of 2 of CD40L) retained all 3 interacting residues. Thus, CD19-deficient and CD40L-deficient patients lack selection against I antigen binding in their immunoglobulin class-switched B cells.

Memory B cells carry on average smaller IgH-CDR3 regions than do naive B cells.[9,37] Indeed, the IgG and IgA transcripts from controls showed smaller IgH-CDR3 sizes (14 aa) than did naive B-cell subsets (17 aa; Fig 4, *C*). The median sizes of IgH-CDR3 in IgA and IgG transcripts in CD19-deficient patients were smaller than in naive B cells, but significantly higher (16 and 15 residues, respectively) than switched transcripts in controls. CD40L-deficient patients showed no reduction in IgH-CDR3 of IgA transcripts.

Together, these findings indicate that in contrast to normal selection for superantigen binding, inherent autoreactivity is not counterselected in CD19-deficient and CD40L-deficient patients.

Targeting and repair of SHMs

To study whether the reduced SHM levels in CD19 and CD40L deficiencies were associated with abnormal targeting and repair, we analyzed mutations in hypermutable motifs and the transition to transversion ratios. In line with previous findings,[22] CD40L-deficient patients showed an increased overall transition over transversion mutation ratio as compared with controls (58/42) (Table I). This was mostly due to transition mutations at C·G (67/33) and significantly increased G→A transitions (see Fig E3 in this article's Online Repository at www.jacionline.org), reminiscent of reduced UNG2 and BER function. Overall targeting of C·G as well as targeting of RGYW/WRCY motifs in CD40L patients seemed unaffected. Targeting of WA/TW motifs was slightly, but not significantly, increased over controls. Together, CD40L-deficient patients show decreased SHM induction by the AID enzyme and decreased UNG2 function in C·G repair, but normal MMR.

Interestingly, CD19-deficient patients showed a decreased transition over the transversion ratio than did controls for both

A

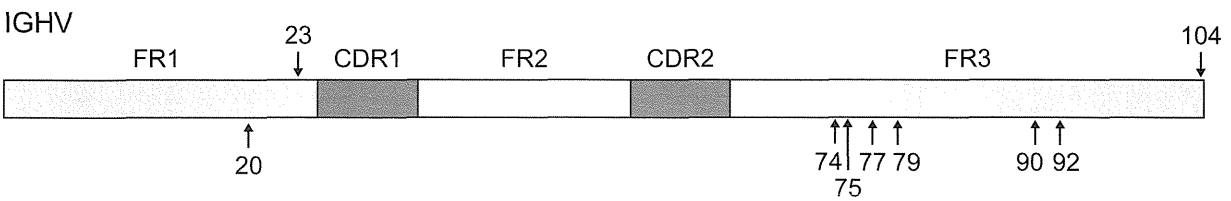

SpA binding residues	20	74	75	77	79	90	92
IGHV3 (n = 22)*	R, *K*	G	R	T	S	Q	N, *G*
IGHV1 (n = 11)*	K	G, *D, E*	R	T	T	E	S, *R*
IGHV4 (n = 11)*	S	S	R	T	S	K	S

* Numbers of IGHV genes in the IGH locus that make up the indicated IGHV subgroup are shown in parentheses; Amino acids in small italics font are represented in less than 10% of functional IGHV subgroup members

B

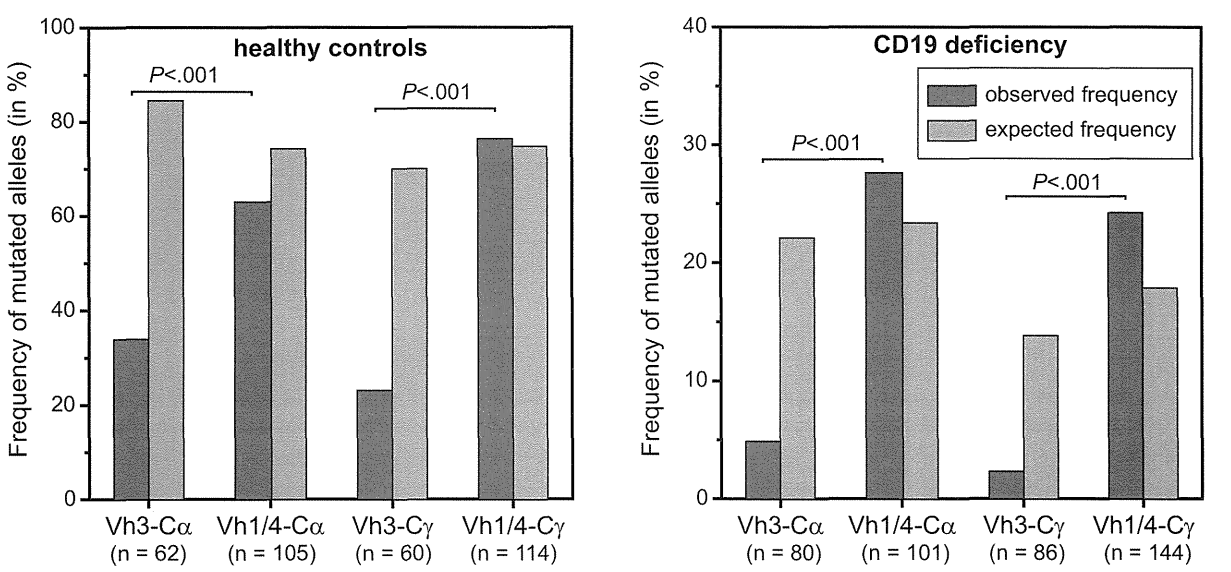

C

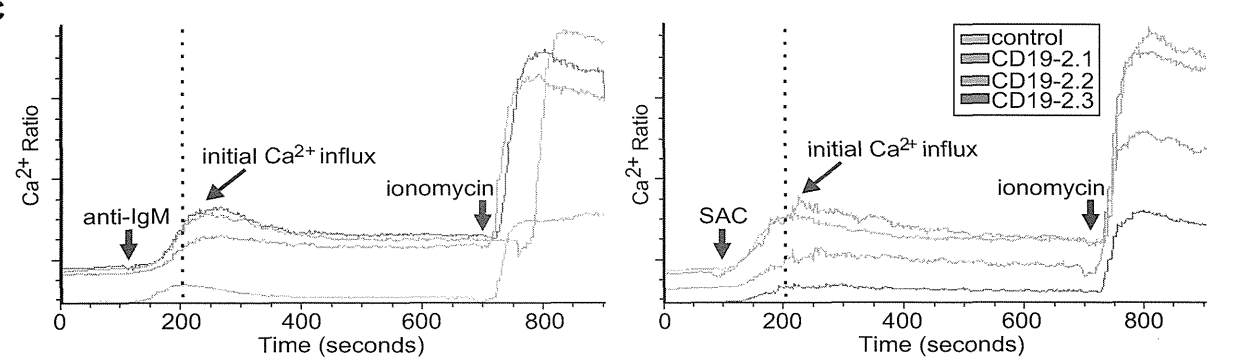

FIG 3. Selection against mutations in SpA-binding residues in *IGHV3* genes of healthy controls and CD19-deficient patients. **A,** Schematic representation of germline-encoded IGHV genes and 7 core residues for SpA binding.[31] **B,** Frequencies of *IGHV* genes with mutations in 1 or more of the 7 core residues for SpA binding. The observed mutation frequencies are shown in *black bars.* The *gray bars* depict the expected mutation frequencies, that is, 7 times the overall mutation frequency of that subset of sequences. Differences in frequencies of mutated *IGHV3* and *IGHV1/4* genes were analyzed with the χ^2 test. **C,** Ca^{2+} influx on B-cell stimulation with anti-IgM or SAC. *SAC, Staphylococcus aureus* Cowan.

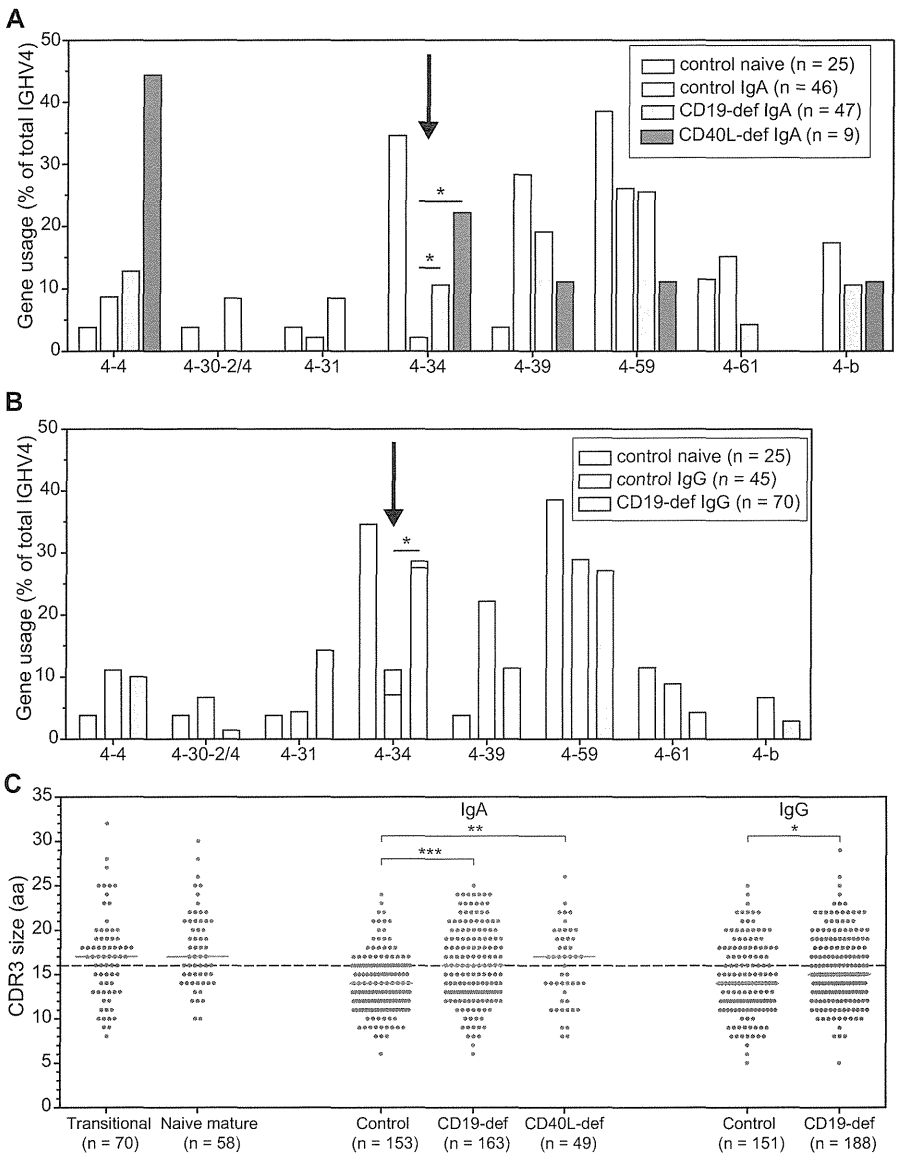

FIG 4. Impaired selection against inherently autoreactive *IGHV4-34* genes and long IgH-CDR3 regions. **A** and **B,** *IGHV4* gene usage in IgA and IgG transcripts. *IGHV4-34* genes with mutations in their I-antigen–binding domain are shown in a *lighter shade.* **C,** IgH-CDR3 sizes of unique transcripts. All individual data points are shown as *gray dots,* with *red lines* indicating the median value. The number of analyzed sequences is indicated in parentheses for each subset. Statistical significance was calculated with the Mann-Whitney test. $*P < .05$; $**P < .01$; and $***P < .001$.

IgG and IgA (Table I). These were partly the result of decreased transitions at C·G, due to decreased G→A transitions and increased C→A transversions (Fig E3), indicative of increased UNG2 and BER activity. Overall targeting was more skewed toward C·G than in healthy controls or CD40L-deficient patients, with normal targeting of WRCY and slightly decreased targeting of RGYW motifs (Table I; also see Table E3 in this article's Online Repository at www.jacionline.org). Furthermore, mutations in WA/TW motifs were reduced, indicating reduced MMR of SHM in CD19-deficiency. Thus, the repair of AID-induced lesions seems differentially affected by the 2 signaling pathways: CD40 signaling is required for UNG2 function, but not for MMR, whereas IgM signaling seems to inhibit BER and favors MMR.

Regulation of AID and error-prone repair genes by IgM and CD40 signaling

To dissect how IgM and CD40 signaling affect SHM induction and repair, we stimulated control naive B cells with anti-IgM, anti-CD40, and IL-4, which supports B-cell survival.[38] Of the previously described genes,[22] *AID*, *UNG2*, MutS-homologues 2 and 6 (*MSH2* and *MSH6*), exonuclease 1 (*EXO1*), and *PCNA* were upregulated after 3 days of culture (Fig 5, *A* and *B*).

Stimulation with anti-IgM in complete absence of anti-CD40 resulted in hardly any upregulation of the studied genes (Fig 5, *C*). Moreover, *RPA1* and *APEX1* were downregulated as compared with unstimulated cells. These effects could not be restored by the addition of B-cell activation stimuli IL-21 or CpG (see Fig E4 in this article's Online Repository at www.jacionline.org).

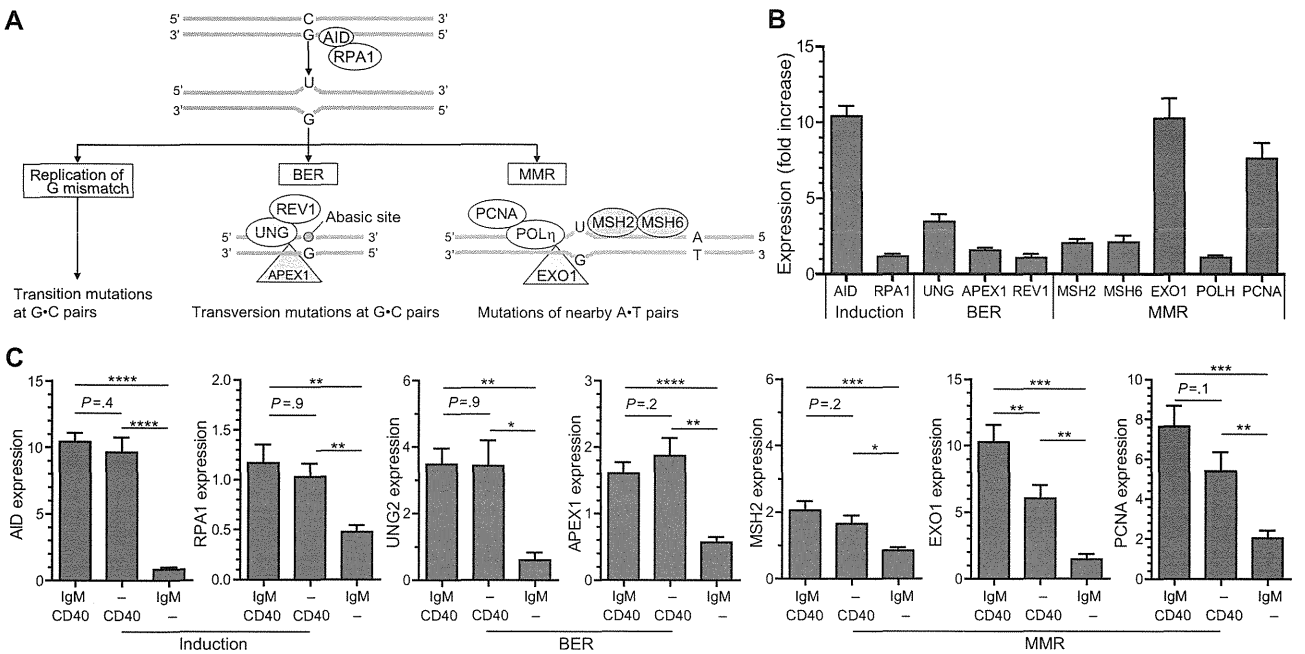

FIG 5. Gene expression levels of SHM targeting and repair genes in activated B cells. **A,** Schematic representation of error-prone repair of AID-induced lesions by replication, BER, or MMR. **B,** Gene expression levels of *AID, RPA1, UNG2, MSH2, MSH6, EXO1, POLH,* and *PCNA* in purified naive B cells from childhood tonsil following stimulation with 10 ng/mL anti-IgM, anti-CD40, and IL-4. **C,** Gene expression levels in the absence of either anti-IgM or anti-CD40 stimulation. The *bars* in (*B*) and (*C*) represent the average fold upregulation of 10 independent donors as compared with unstimulated B cells with SEM error bars. Statistical significance was calculated with the student paired *t* test; $*P < .05$; $**P < .01$; $***P < .001$; and $****P < .0001$. *PCNA,* Proliferating cell nuclear antigen; *POLH,* polymerase η.

The effects on gene expression levels were less severe in the absence of IgM signaling. *AID* was only mildly decreased, and no effects were seen for *RPA1, UNG2,* or *APEX1.* Of the MMR genes, *MSH2, EXO1,* and *PCNA* expression levels were reduced, but not to the extent seen in the absence of CD40. These results confirm the *ex vivo* observations that CD40L-deficient patients, who completely lack CD40 signaling, show strongly decreased AID and UNG2 function. The slight upregulation of *EXO1, MSH6,* and *PCNA* is indicative for residual MMR function of the few lesions created by AID in these patients. IgM signaling was redundant for *UNG2* upregulation but impaired MMR genes. This could explain the observed skewing toward BER over MMR in CD19 deficiency.

DISCUSSION

Here, we analyzed antibody maturation in patients with CD19 and CD40L deficiencies to understand the absence of functional B-cell immunity in these patients. Although selection for superantigen binding was normal in CD19 deficiency, both patient groups showed decreased SHM and reduced selection strengths for antigen binding. Furthermore, selection against inherently autoreactive *IGHV* genes and IGH-CDR3 properties were impaired. Interestingly, SHM targeting and repair were differentially impaired: CD40L-deficient patients displayed reduced UNG2-dependent BER activity, whereas CD19-deficient patients showed increased BER and reduced MMR activity. Thus, the BCR and CD40 signaling pathways together control antibody maturation and selection against autoreactivity.

CD19-deficient and CD40L-deficient patients showed similarly reduced numbers of $CD27^+IgA^+$ and both IgG^+ memory B-cell subsets. This contrasts the much higher serum IgG and IgA levels that can be found in CD19-deficient patients as compared with CD40L-deficient patients. Apparently, the CD19 deficiency drastically impairs circulating B-cell numbers. Although this could result from sequestration in tissue compartments, this likely underlies the lack of a memory response to booster vaccinations seen in CD19-deficient patients.[17] In line with defective secondary responses, IgG2/4 transcript frequencies were strongly reduced in CD19-deficient patients. Immunoglobulin CSR to IgG2/4 frequently occurs via a first switch to IgG1/3. Considering the significantly higher SHM frequencies in IgG2 than in IgG1/3 transcripts, indirect switching to IgG2 does take place in CD19-deficient patients, but to a much smaller extent than in healthy individuals.

CD19-deficient patients had more severely reduced $CD27^+IgM^+IgD^+$ natural effector B-cell numbers than did CD40L-deficient patients. In the absence of CD40 signaling and functional GCs, these cells are thought to be derived from the splenic marginal zone, while in healthy controls these might be a mixture of GC and marginal zone–derived B cells. The low numbers of circulating natural effector cells in CD19-deficient patients indicate that both differentiation pathways are affected, suggesting a crucial role for IgM signaling in both GC and marginal zone responses. Both CD19-deficient and CD40L-deficient patients showed normal numbers of $CD27^-IgA^+$ B cells, indicating normal formation of memory from local mucosal tissue. Still, their SHM levels and selection for replacement

mutations in IGHV-CDR were impaired, and the patients displayed reduced use of the IgA2 subclass, which is resistant to bacterial proteases. Thus, despite seemingly normal numbers, local mucosal IgA responses are qualitatively impaired in the absence of CD40 or CD19-dependent BCR signaling.

The strongly reduced SHM frequencies in CD19-deficient and CD40L-deficient patients provide little sequence variation for the subsequent selection of high-affinity receptors. This could be the basis for the reduced selection strength in immunoglobulin-switched transcripts of the patients. Moreover, the selection processes against inherently autoreactive features of IgH, long CDR3 and IGHV4-34 were absent. The defects seemed more severe in CD40L-deficient patients than in CD19-deficient patients. This could be due to the impaired upregulation of AID, which is required for human B-cell tolerance.[39] Alternatively, it could reflect either the importance of CD40 signaling over BCR signaling, or, more likely, residual BCR signaling in the absence of CD19.

CD19-deficient patients showed normal Ca^{2+} responses to *S aureus* Cowan and normal selection against mutations in SpA-binding residues in the FR. Thus, CD19 seems redundant in the response to this superantigen. It has been disputed whether the binding of SpA to IGHV3 induces immune responses or B-cell death.[40] This is most likely dependent on the local environment, because IL-4 and CD40L protect B cells from SpA-induced apoptosis.[40] Our findings that in healthy individuals SpA-binding residues are selectively unmutated indicate that there are selection processes *in vivo* to retain SpA superantigen binding. It appears that the maintenance of a large population of antigen-experienced B cells capable of SpA binding is favorable for the host.

CD19 deficiency showed a unique SHM targeting profile with decreased transition mutations and increased MMR, which, to our knowledge, has not been described before. Rather, deficiencies in DNA repair genes result in increased transition mutations (UNG, MSH2, MSH6, and EXO1 deficiencies),[41-46] or in increased G·C targeting (polymerase η and proliferating cell nuclear antigen deficiencies).[47-50] Our *in vitro* studies indicated that BCR signaling was needed to upregulate MMR genes, but not UNG2 and APEX1. This contrasts CD40L deficiency that impaired both BER and MMR. Thus, CD19-dependent BCR signaling seems to specifically affect MMR at the transcriptional level, although the exact mechanism behind this remains to be elucidated.

IgA transcripts of CD40L-deficient patients had few mutations, which showed signs of reduced UNG2 activity at G·C, but normal MMR as evidenced by the normal A·T targeting. These observations were mostly in line with published data on SHM targeting in $CD27^+IgM^+IgD^+$ B cells of CD40L-deficient patients.[22] In contrast to this report, we observed normal targeting of G residues in RGYW motifs, and higher SHM levels in IgA transcripts, suggestive of more AID activity. This could be inherent to IgA responses, because in healthy controls also, IgA^+ memory B cells show higher levels of SHM than do IgM^+ or IgG^+ memory B-cell subsets.[9] Our results support other observations of CD40-independent SHM and CSR in intestinal mucosa through TACI and Toll-like receptor signaling.[12-14] However, these processes are unable to upregulate AID and UNG2 levels to the same extent as CD40. Moreover, GC-independent $CD27^-IgA^+$ memory B cells in healthy controls show increased SHM, transversion mutations, and IgA2 CSR,[9] indicative of higher AID and UNG2 activity than in CD40L deficiency. Thus, it remains possible that in healthy controls CD40 signaling is directly or indirectly involved in generating their antigen-experienced repertoire.

In conclusion, BCR and CD40 signals are required for AID-induced DNA breaks, affinity maturation, and selection against inherently autoreactive features, whereas these signals skew DNA break repair: CD40 signaling promotes BER, and BCR-CD19 signaling promotes MMR. Thus, the human antigen–experienced B-cell repertoire is shaped *in vivo* through balanced signaling via the BCR and CD40 to ensure optimal affinity maturation and selection against autoreactivity. These new insights from well-defined human inherited disorders provide means to study antibody maturation and selection defects in patients with immune-mediated diseases, including primary immunodeficiencies and autoimmune disorders.

We thank Mrs S. de Bruin-Versteeg for assistance with the figures, and Drs E. Meffre and J. E. Guikema for critical reading of the manuscript.

Key messages

- **Memory B cells in patients with CD19 or CD40L deficiency are impaired not only in numbers but also in the quality of their antibodies.**
- **B-cell antigen receptor and CD40 signaling balance the 2 DNA repair mechanisms involved in affinity maturation of antibodies.**
- **Impaired antibody selection in patients with B-cell antigen receptor signaling defects might underlie their autoimmunity.**

REFERENCES

1. Alt FW, Yancopoulos GD, Blackwell TK, Wood C, Thomas E, Boss M, et al. Ordered rearrangement of immunoglobulin heavy chain variable region segments. Embo J 1984;3:1209-19.
2. Rajewsky K, Forster I, Cumano A. Evolutionary and somatic selection of the antibody repertoire in the mouse. Science 1987;238:1088-94.
3. Stavnezer J, Guikema JE, Schrader CE. Mechanism and regulation of class switch recombination. Annu Rev Immunol 2008;26:261-92.
4. Liu M, Schatz DG. Balancing AID and DNA repair during somatic hypermutation. Trends Immunol 2009;30:173-81.
5. Saribasak H, Gearhart PJ. Does DNA repair occur during somatic hypermutation? Semin Immunol 2012;24:287-92.
6. Xu Z, Zan H, Pone EJ, Mai T, Casali P. Immunoglobulin class-switch DNA recombination: induction, targeting and beyond. Nat Rev Immunol 2012;12:517-31.
7. Muramatsu M, Kinoshita K, Fagarasan S, Yamada S, Shinkai Y, Honjo T. Class switch recombination and hypermutation require activation-induced cytidine deaminase (AID), a potential RNA editing enzyme. Cell 2000;102:553-63.
8. Durandy A, Kracker S, Fischer A. Primary antibody deficiencies. Nat Rev Immunol 2013;13:519-33.
9. Berkowska MA, Driessen GJ, Bikos V, Grosserichter-Wagener C, Stamatopoulos K, Cerutti A, et al. Human memory B cells originate from three distinct germinal center-dependent and -independent maturation pathways. Blood 2011;118:2150-8.
10. He B, Xu W, Santini PA, Polydorides AD, Chiu A, Estrella J, et al. Intestinal bacteria trigger T cell-independent immunoglobulin A(2) class switching by inducing epithelial-cell secretion of the cytokine APRIL. Immunity 2007;26:812-26.
11. Weller S, Faili A, Garcia C, Braun MC, Le Deist FF, de Saint Basile GG, et al. CD40-CD40L independent Ig gene hypermutation suggests a second B cell diversification pathway in humans. Proc Natl Acad Sci U S A 2001;98:1166-70.
12. Gourzi P, Leonova T, Papavasiliou FN. Viral induction of AID is independent of the interferon and the Toll-like receptor signaling pathways but requires NF-kappaB. J Exp Med 2007;204:259-65.

13. He B, Qiao X, Cerutti A. CpG DNA induces IgG class switch DNA recombination by activating human B cells through an innate pathway that requires TLR9 and cooperates with IL-10. J Immunol 2004;173:4479-91.
14. He B, Santamaria R, Xu W, Cols M, Chen K, Puga I, et al. The transmembrane activator TACI triggers immunoglobulin class switching by activating B cells through the adaptor MyD88. Nat Immunol 2010;11:836-45.
15. Lam KP, Kuhn R, Rajewsky K. In vivo ablation of surface immunoglobulin on mature B cells by inducible gene targeting results in rapid cell death. Cell 1997;90:1073-83.
16. Srinivasan L, Sasaki Y, Calado DP, Zhang B, Paik JH, DePinho RA, et al. PI3 kinase signals BCR-dependent mature B cell survival. Cell 2009;139:573-86.
17. van Zelm MC, Reisli I, van der Burg M, Castaño D, van Noesel CJM, van Tol MJD, et al. An antibody-deficiency syndrome due to mutations in the CD19 gene. N Engl J Med 2006;354:1901-12.
18. van Zelm MC, Smet J, Adams B, Mascart F, Schandene L, Janssen F, et al. CD81 gene defect in humans disrupts CD19 complex formation and leads to antibody deficiency. J Clin Invest 2010;120:1265-74.
19. van Zelm MC, Smet J, van der Burg M, Ferster A, Le PQ, Schandene L, et al. Antibody deficiency due to a missense mutation in CD19 demonstrates the importance of the conserved tryptophan 41 in immunoglobulin superfamily domain formation. Hum Mol Genet 2011;20:1854-63.
20. Engel P, Zhou LJ, Ord DC, Sato S, Koller B, Tedder TF. Abnormal B lymphocyte development, activation, and differentiation in mice that lack or overexpress the CD19 signal transduction molecule. Immunity 1995;3:39-50.
21. Rickert RC, Rajewsky K, Roes J. Impairment of T-cell-dependent B-cell responses and B-1 cell development in CD19-deficient mice. Nature 1995;376:352-5.
22. Longo NS, Lugar PL, Yavuz S, Zhang W, Krijger PH, Russ DE, et al. Analysis of somatic hypermutation in X-linked hyper-IgM syndrome shows specific deficiencies in mutational targeting. Blood 2009;113:3706-15.
23. Artac H, Reisli I, Kara R, Pico-Knijnenburg I, Adin-Cinar S, Pekcan S, et al. B-cell maturation and antibody responses in individuals carrying a mutated CD19 allele. Genes Immun 2010;11:523-30.
24. Kanegane H, Agematsu K, Futatani T, Sira MM, Suga K, Sekiguchi T, et al. Novel mutations in a Japanese patient with CD19 deficiency. Genes Immun 2007;8:663-70.
25. Alamyar E, Duroux P, Lefranc MP, Giudicelli V. IMGT(®) tools for the nucleotide analysis of immunoglobulin (IG) and T cell receptor (TR) V-(D)-J repertoires, polymorphisms, and IG mutations: IMGT/V-QUEST and IMGT/HighV-QUEST for NGS. Methods Mol Biol 2012;882:569-604.
26. Uduman M, Yaari G, Hershberg U, Stern JA, Shlomchik MJ, Kleinstein SH. Detecting selection in immunoglobulin sequences. Nucleic Acids Res 2011;39:W499-504.
27. Brezinschek HP, Brezinschek RI, Lipsky PE. Analysis of the heavy chain repertoire of human peripheral B cells using single-cell polymerase chain reaction. J Immunol 1995;155:190-202.
28. Suzuki I, Pfister L, Glas A, Nottenburg C, Milner EC. Representation of rearranged VH gene segments in the human adult antibody repertoire. J Immunol 1995;154:3902-11.
29. Chang B, Casali P. The CDR1 sequences of a major proportion of human germline Ig VH genes are inherently susceptible to amino acid replacement. Immunol Today 1994;15:367-73.
30. Yaari G, Uduman M, Kleinstein SH. Quantifying selection in high-throughput immunoglobulin sequencing data sets. Nucleic Acids Res 2012;40:e134.
31. Graille M, Stura EA, Corper AL, Sutton BJ, Taussig MJ, Charbonnier JB, et al. Crystal structure of a *Staphylococcus aureus* protein A domain complexed with the Fab fragment of a human IgM antibody: structural basis for recognition of B-cell receptors and superantigen activity. Proc Natl Acad Sci U S A 2000;97:5399-404.
32. Kristiansen SV, Pascual V, Lipsky PE. Staphylococcal protein A induces biased production of Ig by VH3-expressing B lymphocytes. J Immunol 1994;153:2974-82.
33. Scharenberg AM, Kinet JP. PtdIns-3,4,5-P3: a regulatory nexus between tyrosine kinases and sustained calcium signals. Cell 1998;94:5-8.
34. Rao SP, Riggs JM, Friedman DF, Scully MS, LeBien TW, Silberstein LE. Biased VH gene usage in early lineage human B cells: evidence for preferential Ig gene rearrangement in the absence of selection. J Immunol 1999;163:2732-40.
35. Yu K, Taghva A, Lieber MR. The cleavage efficiency of the human immunoglobulin heavy chain VH elements by the RAG complex: implications for the immune repertoire. J Biol Chem 2002;277:5040-6.
36. Potter KN, Hobby P, Klijn S, Stevenson FK, Sutton BJ. Evidence for involvement of a hydrophobic patch in framework region 1 of human V4-34-encoded Igs in recognition of the red blood cell I antigen. J Immunol 2002;169:3777-82.
37. Wu YC, Kipling D, Leong HS, Martin V, Ademokun AA, Dunn-Walters DK. High-throughput immunoglobulin repertoire analysis distinguishes between human IgM memory and switched memory B-cell populations. Blood 2010;116:1070-8.
38. Foote LC, Howard RG, Marshak-Rothstein A, Rothstein TL. IL-4 induces Fas resistance in B cells. J Immunol 1996;157:2749-53.
39. Meyers G, Ng YS, Bannock JM, Lavoie A, Walter JE, Notarangelo LD, et al. Activation-induced cytidine deaminase (AID) is required for B-cell tolerance in humans. Proc Natl Acad Sci U S A 2011;108:11554-9.
40. Goodyear CS, Silverman GJ. Death by a B cell superantigen: in vivo VH-targeted apoptotic supraclonal B cell deletion by a Staphylococcal toxin. J Exp Med 2003;197:1125-39.
41. Bardwell PD, Woo CJ, Wei K, Li Z, Martin A, Sack SZ, et al. Altered somatic hypermutation and reduced class-switch recombination in exonuclease 1-mutant mice. Nat Immunol 2004;5:224-9.
42. Gardes P, Forveille M, Alyanakian MA, Aucouturier P, Ilencikova D, Leroux D, et al. Human MSH6 deficiency is associated with impaired antibody maturation. J Immunol 2012;188:2023-9.
43. Phung QH, Winter DB, Cranston A, Tarone RE, Bohr VA, Fishel R, et al. Increased hypermutation at G and C nucleotides in immunoglobulin variable genes from mice deficient in the MSH2 mismatch repair protein. J Exp Med 1998;187:1745-51.
44. Rada C, Williams GT, Nilsen H, Barnes DE, Lindahl T, Neuberger MS. Immunoglobulin isotype switching is inhibited and somatic hypermutation perturbed in UNG-deficient mice. Curr Biol 2002;12:1748-55.
45. Wiesendanger M, Kneitz B, Edelmann W, Scharff MD. Somatic hypermutation in MutS homologue (MSH)3-, MSH6-, and MSH3/MSH6-deficient mice reveals a role for the MSH2-MSH6 heterodimer in modulating the base substitution pattern. J Exp Med 2000;191:579-84.
46. Imai K, Slupphaug G, Lee WI, Revy P, Nonoyama S, Catalan N, et al. Human uracil-DNA glycosylase deficiency associated with profoundly impaired immunoglobulin class-switch recombination. Nat Immunol 2003;4:1023-8.
47. Yavuz S, Yavuz AS, Kraemer KH, Lipsky PE. The role of polymerase eta in somatic hypermutation determined by analysis of mutations in a patient with xeroderma pigmentosum variant. J Immunol 2002;169:3825-30.
48. Delbos F, Aoufouchi S, Faili A, Weill JC, Reynaud CA. DNA polymerase eta is the sole contributor of A/T modifications during immunoglobulin gene hypermutation in the mouse. J Exp Med 2007;204:17-23.
49. Wilson TM, Vaisman A, Martomo SA, Sullivan P, Lan L, Hanaoka F, et al. MSH2-MSH6 stimulates DNA polymerase eta, suggesting a role for A:T mutations in antibody genes. J Exp Med 2005;201:637-45.
50. Roa S, Avdievich E, Peled JU, Maccarthy T, Werling U, Kuang FL, et al. Ubiquitylated PCNA plays a role in somatic hypermutation and class-switch recombination and is required for meiotic progression. Proc Natl Acad Sci U S A 2008;105:16248-53.

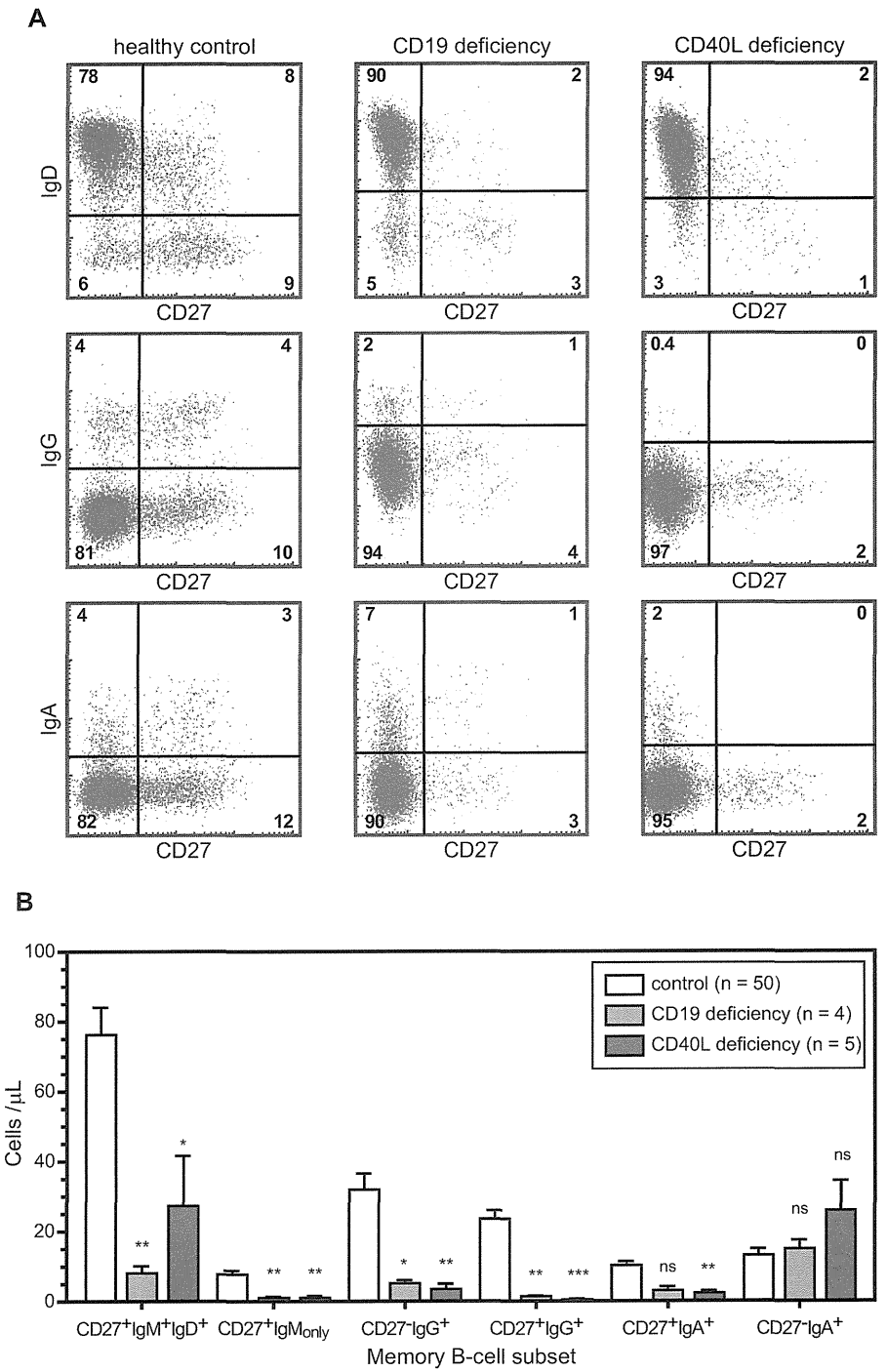

FIG E1. Memory B cells in CD19-deficient and CD40L-deficient patients. **A,** Representative FACS plots. **B,** Absolute cell numbers of 6 memory B-cell subsets (mean ± SEM). Data included from patients XHIM-1.2, XHIM-1.3, XHIM-9, XHIM-11, and XHIM-12, CD19-1.1, CD19-1.2, and CD19-4, and CD81-1. Statistical significance was calculated with the Mann-Whitney test: *ns*, Not significant; $^{*}P < .05$; $^{**}P < .01$; and $^{***}P < .001$. *FACS*, Fluorescence-activated cell sorting.

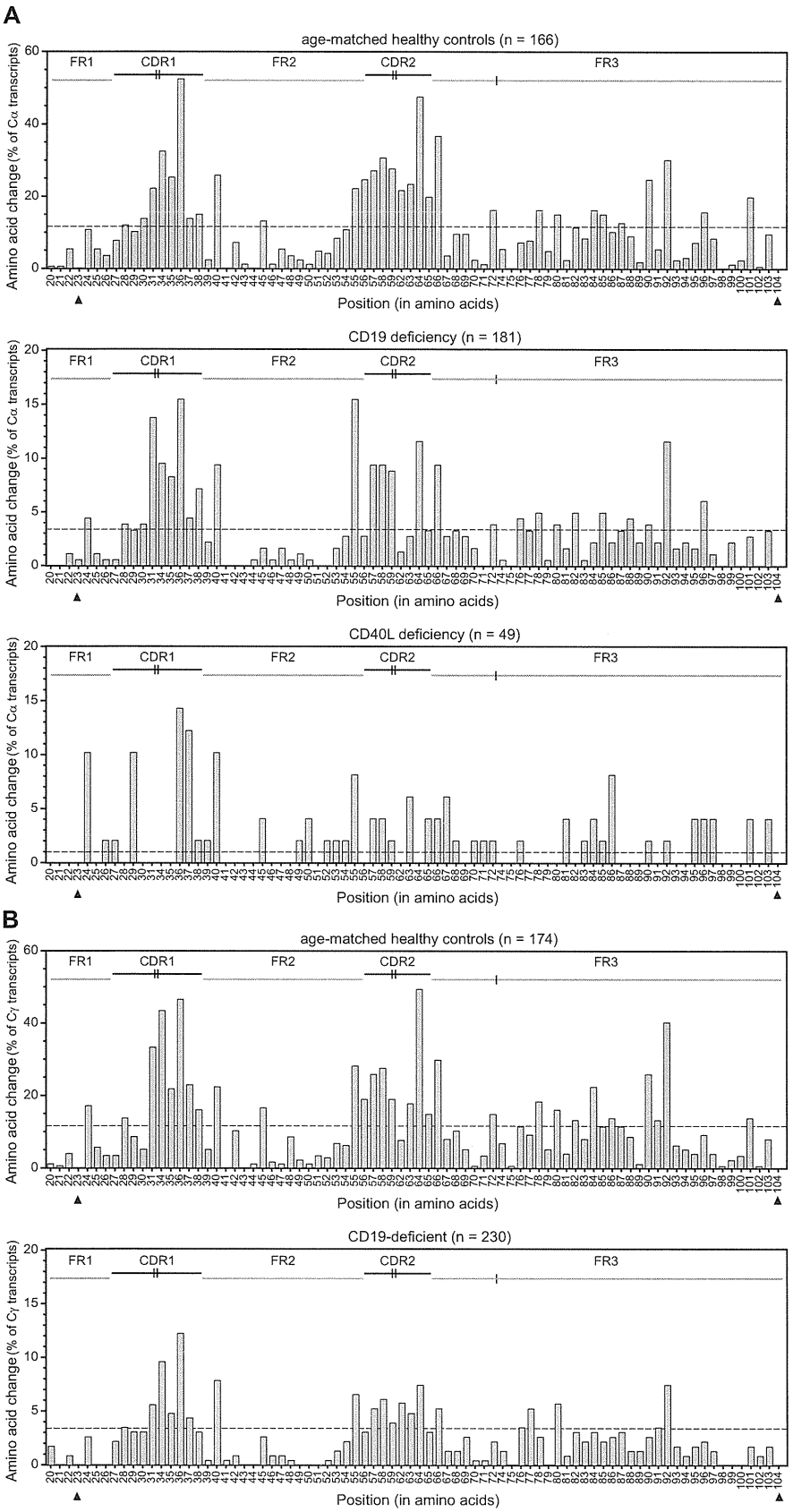

FIG E2. Distribution of amino acid replacements in rearranged *IGHV* genes. Distribution of amino acid replacements in rearranged *IGHV* genes derived from sequence analysis of **(A)** Cα transcripts and **(B)** Cγ

Control IgG Absolute numbers

To / From	A	C	G	T	
A		196	398	173	767
C	119		241	410	770
G	487	329		204	1020
T	110	221	102		433
					2990

Frequencies

To / From	A	C	G	T	
A		6.6	13.3	5.8	25.7
C	4.0		8.1	13.7	25.8
G	16.3	11.0		6.8	34.1
T	3.7	7.4	3.4		14.5
					100

CD19 IgG Absolute numbers

To / From	A	C	G	T	
A		82	158	88	328
C	109 *		124	167	400
G	217 *	155		166 *	538
T	55	99	73 *		227
					1493

Frequencies

To / From	A	C	G	T	
A		5.5	10.6	5.9	22.0
C	7.3		8.3	11.2	26.8
G	14.5	10.4		11.1	36.0
T	3.7	6.6	4.9		15.2
					100

Control IgA Absolute numbers

To / From	A	C	G	T	
A		164	361	174	699
C	97		203	378	678
G	431	306		197	934
T	85	224	105		414
					2725

Frequencies

To / From	A	C	G	T	
A		6.0	13.2	6.4	25.7
C	3.6		7.4	13.9	24.9
G	15.8	11.2		7.2	34.3
T	3.1	8.2	3.9		15.2
					100

CD19 IgA Absolute numbers

To / From	A	C	G	T	
A		65	126 *	120 *†	311
C	92 *†		121	246 †	459
G	213 *	171		162 *	546
T	64 *	87 *	65		216
					1532

Frequencies

To / From	A	C	G	T	
A		4.2	8.2	7.8	20.3
C	6.0		7.9	16.1	30.0
G	13.9	11.2		10.6	35.6
T	4.2	5.7	4.2		14.1
					100

CD40L IgA Absolute numbers

To / From	A	C	G	T	
A		10	21 *	8 ‡	39
C	4		13	22	39
G	40 *‡	14		6 *‡	60
T	12	20	7		39
					177

Frequencies

To / From	A	C	G	T	
A		5.6	11.9	4.5	22.0
C	2.3		7.3	12.4	22.0
G	22.6	7.9		3.4	33.9
T	6.8	11.3	4.0		22.0
					100

FIG E3. Substitution of individual nucleotides in rearranged *IGHV*. Individual nucleotide substitutions for IgG rearrangements of controls and CD19-deficient patients and IgA rearrangements cells of controls, CD19-deficient patients, and CD40L-deficient patients are given both in absolute number *(left panels)* and in relative frequencies *(right panels)*. The number of analyzed sequences is similar as in Table I and Table E2. All analyses were performed with the JoinSolver program and statistically analyzed with the χ^2 test. Significant differences are indicated with an *asterisk* between patient and control cells, with a hash between IgG and IgA of controls, with a single dagger between IgG and IgA of CD19 deficiency, and with a *double dagger* between IgA of CD19 and CD40L deficiency.

transcripts from healthy controls, CD19-deficient patients, and CD40L-deficient patients. The number of analyzed sequences is indicated in parentheses. Each *bar* represents the frequency of substitutions at each amino acid position starting from 20 (first codon following primer sequence) to 104 (last codon of the FR3). *Horizontal dotted lines* indicate average replacement mutation frequencies; *triangles* indicate conserved cysteines: first CYS-23 and second CYS-104.

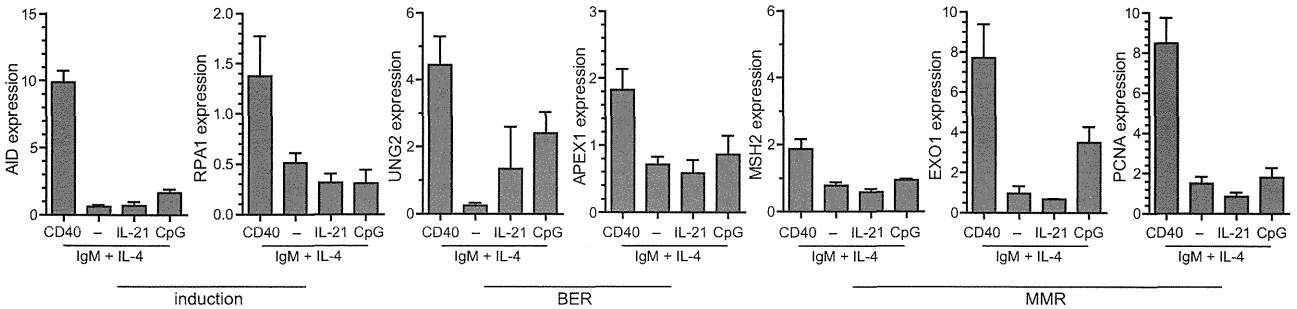

FIG E4. Gene expression levels of SHM targeting and repair genes in IgM + IL-4 activated B cells with CD40, IL-21, or CpG costimulation. The *bars* represent the average fold upregulation of 4 independent donors as compared with unstimulated B cells with SEM error bars.

TABLE E1. Patients with absence of CD19 or CD40L protein expression

Patient	Age (y); sex	Gene	Mutation		Membrane expression			Serum immunoglobulin (mg/dL)			Reference
			cDNA	Protein	CD19	CD81	CD40L	IgG	IgA	IgM	
CD19-1.1	10; F	*CD19*	c.972insA	p.Arg325AlafsX4	−	+	ND	**325**	292	**25**	17
CD19-1.2	12; M	*CD19*	c.972insA	p.Arg325AlafsX4	−	+	ND	**91**	**1**	59	23
CD19-2.1	35; M	*CD19*	c.1384delGA	p.Asn463ArgfsX3	−	+	ND	**204**	**18**	**47**	17
CD19-2.2	33; F	*CD19*	c.1384delGA	p.Asn463ArgfsX3	−	+	ND	**198**	**7**	**30**	17
CD19-2.3	49; F	*CD19*	c.1384delGA	p.Asn463ArgfsX3	−	+	ND	**256**	**19**	63	17
CD19-3	8; M	*CD19*	c.947-1G>T; gene deletion	p.Ala316Asp fsX5; p.X	−	+	ND	**249**	**10**	**18**	24
CD19-4	6; F	*CD19*	c.G156C	p.Trp52Cys	−	+	ND	**300**	50	**40**	19
CD81-1	4; F	*CD81*	c.561+1G>A	p.Glu188MetfsX13	−	−	ND	**240**	71	**35**	18
XHIM-1.2	13; M	*CD40L*	c.761C>T	p.Thr254Met	+	ND	−	**115**	**<20**	124	9
XHIM-1.3	1; M	*CD40L*	c.761C>T	p.Thr254Met	+	ND	−	**80**	**<1**	**<30**	9
XHIM-2	3; M	*CD40L*	c.617T>C	p.Leu206Pro	+	ND	−	**23**	**35**	139	
XHIM-7.1	3; M	*CD40L*	c.662A>C	p.Gln221Pro	+	ND	−	**<20**	**<7**	306	
XHIM-9	2; M	*CD40L*	c.474delG	p.Gly158fsX4	+	ND	−	**80**	47	154	9
XHIM-10	4; M	*CD40L*	c.435delC	p.Tyr146ThrfsX3	+	ND	−	**<134**	**<6**	71	
XHIM-11	1; M	*CD40L*	c.154A>T	p.Lys52X	+	ND	−	**152**	**6**	178	9
XHIM-12	1; M	*CD40L*	c.521A>C	p.Gln174Pro	+	ND	−	**92**	**<6**	121	9

Subnormal values as compared with age-matched controls are shown in boldface. *F*, Female; *M*, male.

TABLE E2. PCR primers and UPL FAM-labeled hydrolysis probes for gene expression analysis

Gene	Forward primer (5′-3′)	Position (exon)	Reverse primer (5′-3′)	Position (exon)	UPL probe no.
AID	ACTCTGGACACCACTATGGACA	1	GCGGACATTTTTGAATTGGT	2	69
APEX1	GCTTCGAGCCTGGATTAAGA	3	TTGGTCTCTTGAAGGCACAGT	4	45
EXO1	TGAGCTCTGGAAAAACTTTGG	15	CTGGGGACAGGGGTTTCT	16	69
MSH2	CAAGGAGAATGATTGGTATTTGG	2	CCAAAGAGAATGTCTTCAAACTGAG	3	2
MSH6	AAGGCGAAGAACCTCAACG	1	CTGGTGAGAAGTCACAACTGGT	2	40
PCNA	TGGAGAACTTGGAAATGGAAA	4	GAACTGGTTCATTCATCTCTATGG	5	69
POLH	TGAATCCCAGCTCCAGAGTC	7	GCCTGGGTTTAACTGGATCA	8	7
REV1	CAATTTTTAGTGGAGTTGCCATC	3	CCTCCATGCAACATCATTAGTTT	4	73
RPA1	TGCCCTATAATGAAGGACTCG	5	GAACCCATTCCCGAGCTT	7	3
UNG2	TGAGGAAAGCGGAGATGC	1	GATCCGGTCCAACTGCTC	2	51

FAM, Fluorescein; *PCNA*, proliferating cell nuclear antigen; *POLH*, polymerase η; *UPL*, universal probe library.

TABLE E3. Targeting of individual nucleotides in hypermutable motifs

	IgA						IgG					
	Control (n = 153)		CD19-deficient (n = 202)		CD40L-deficient (n = 50)		Control (n = 163)		CD19-deficient (n = 221)			
G												
Inside RGYW	364.5/1439 (25.3)	**4.1**	157.5/1936 (8.1)	**2.6**	25/437.5 (5.7)	**5.2**	434/1518.5 (28.6)	**4.8**	132/2105.7 (6.3)	**2.2**		
All other G	569.5/9241 (6.2)		388.5/12543 (3.1)		35/3072.5 (1.1)		586/9758.5 (6.0)		406/14002.3 (2.9)			
C												
Inside WRCY	229.8/1267.7 (18.1)	**3.8**	135.5/1693 (8.0)	**3.1**	11/397.5 (2.7)	**2.5**	259.1/1301.7 (19.9)	**3.9**	98/1965.5 (5.0)	**2.3**		
All other C	448.2/9397.3 (4.8)		323.5/12457 (2.6)		28/2657.5 (1.1)		510.9/9919.3 (5.2)		302/14024.4 (2.2)			
A												
Inside WA	332/2249.5 (14.8)	**2.6**	126/3032 (4.2)	**2.0**	23/798.5 (2.9)	**3.6**	367.5/2391.5 (15.4)	**2.6**	115.1/3349.7 (3.4)	**1.6**		
All other A	367/6452.5 (5.7)		185/8740 (2.1)		16/2116.5 (0.8)		399.5/6773.5 (5.9)		212.8/9826.3 (2.2)			
T												
Inside TW	202.5/1724 (11.7)	**3.6**	92/2505 (3.7)	**2.6**	23/604.5 (3.8)	**4.7**	201.8/1820.8 (11.1)	**3.3**	78.5/2721.7 (2.9)	**1.9**		
All other T	211.5/6483 (3.3)		124/8709 (1.4)		16/1987.5 (0.8)		231.3/6889.3 (3.4)		148.5/9761.3 (1.5)			
A												
Inside RGYW	127.5/649 (19.6)	**2.8**	48/1006.5 (4.8)	**2.0**	6.5/249 (2.6)	**2.1**	159/735 (21.6)	**3.0**	53/1061 (5.0)	**2.2**		
All other A	571.5/8053 (7.1)		263/10765.5 (2.4)		32.5/2666 (1.2)		608/8430 (7.2)		275/12115 (2.3)			
A												
Inside WRCY	94.5/1174 (8.0)	**1.0**	33/1430.5 (2.3)	**0.9**	3.5/266 (1.3)	**1.0**	105/1209 (8.7)	**1.0**	48/1797 (2.7)	**1.1**		
All other A	604.5/7528 (8.0)		278/10341.5 (2.7)		35.5/2649 (1.3)		662/7956 (8.3)		280/11379 (2.5)			

The number of underlined (commonly mutated) nucleotides inside and outside the motifs was calculated with the JoinSolver software (frequency in parentheses). The ratio between the frequency of mutations inside and outside the motifs is depicted in boldface and used as a measurement of targeting. The number of analyzed sequences is indicated in parentheses next to the name of each population.

Molecular Immunology 58 (2014) 66–76

Contents lists available at ScienceDirect

Molecular Immunology

journal homepage: www.elsevier.com/locate/molimm

Functional assessment of the mutational effects of human *IRAK4* and *MyD88* genes

Takahiro Yamamoto[a,1], Naotaka Tsutsumi[b,1], Hidehito Tochio[b,**], Hidenori Ohnishi[a,*], Kazuo Kubota[a], Zenichiro Kato[a], Masahiro Shirakawa[b,c], Naomi Kondo[a,d]

[a] Department of Pediatrics, Graduate School of Medicine, Gifu University, 1-1 Yanagido, Gifu 501-1194, Japan
[b] Department of Molecular Engineering, Graduate School of Engineering, Kyoto University, Katsura, Nishikyo-ku, Kyoto 615-8510, Japan
[c] Core Research for Evolutional Science and Technology, Japan Science and Technology Corporation, 4-1-8 Hon-cho, Kawaguchi, Saitama 332-0012, Japan
[d] Heisei College of Health Sciences, 180 Kurono, Gifu 501-1131, Japan

ARTICLE INFO

Article history:
Received 3 October 2013
Received in revised form 8 November 2013
Accepted 9 November 2013
Available online 5 December 2013

Keywords:
IRAK4
MyD88
Myddosome
TIR domain
Death domain
Immune-deficiency

ABSTRACT

Human interleukin-1 receptor-associated kinase 4 (IRAK4) deficiency and myeloid differentiating factor 88 (MyD88) deficiency syndromes are two primary immune-deficiency disorders with innate immune defects. Although new genetic variations of *IRAK4* and *MyD88* have recently been deposited in the single nucleotide polymorphism (SNP) database, the clinical significance of these variants has not yet been established. Therefore, it is important to establish methods for assessing the association of each gene variation with human diseases. Because cell-based assays, western blotting and an NF-κB reporter gene assay, showed no difference in protein expression and NF-κB activity between R12C and wild-type IRAK4, we examined protein–protein interactions of purified recombinant IRAK4 and MyD88 proteins by analytical gel filtration and NMR titration. We found that the variant of IRAK4, R12C, as well as R20W, located in the death domain of IRAK4 and regarded as a SNP, caused a loss of interaction with MyD88. Our studies suggest that not only the loss of protein expression but also the defect of Myddosome formation could cause IRAK4 and MyD88 deficiency syndromes. Moreover a combination of *in vitro* functional assays is effective for confirming the pathogenicity of mutants found in IRAK4 and MyD88-deficiency patients.

1. Introduction

Interleukin-1 receptor-associated kinase (IRAK) 4 is the one of the essential molecules of the Toll/interleukin-1 receptor signaling pathway (Suzuki et al., 2002). In this pathway, ligand-induced hetero- or homodimerization of receptors recruits the Toll/interleukin-1 receptor homology domain (TIR domain) containing adaptor oligomers. One of these adaptors, MyD88, then binds IRAK4 (Burns et al., 2003). Recently, defects in the innate immune system have been shown to cause newly categorized human primary immune-deficiency syndromes (Al-Herz et al., 2011) such as human IRAK4 deficiency (Picard et al., 2003).

In affected IRAK4 deficient patients, invasive infections such as bacterial meningitis, sepsis, arthritis, or osteomyelitis are caused by *Streptococcus pneumonia*, *Staphylococcus aureus*, and *Pseudomonas aeruginosa* (Picard et al., 2010). Human MyD88 deficiency (von Bernuth et al., 2008) has remarkably similar clinical features to human IRAK4 deficiency. Interestingly, the life-threatening infections in IRAK4 or MyD88 deficient patients first occur during early infancy, but their frequency and severity reduce after the teenage years (Picard et al., 2011). Therefore, it is necessary for them to be diagnosed quickly.

IRAK4 and MyD88 proteins both consist of two major functional domains. In IRAK4, the death domain (DD) interacts with MyD88, while the kinase domain phosphorylates downstream signaling factors such as IRAK1, IRAK2, and subsequently causes activation of TNF Receptor Associated Factor 6 (TRAF6). In MyD88, both the DD and TIR domains interact in homotypic binding to similar domain structures. The domain–domain interactions are critical for these signaling pathways. IRAK4 and MyD88 form a hetero-oligomeric signaling complex via a shared DD, so-called Myddosome (Motshwene et al., 2009). Appropriate Myddosome

Abbreviations: DD, death domain; HEK, human embryonic kidney; ID, internal domain; IRAK, Interleukin-1 receptor-associated kinase; MyD88, myeloid differentiating factor 88; Mal, MyD88 adaptor-like; NMR, nuclear magnetic resonance; ELISA, enzyme-linked immunosorbent assay; TIR domain, Toll/interleukin-1 receptor homology domain; WT, wild type; SNP, single nucleotide polymorphism; IRAK4-DD, death domain of IRAK4; IRAK4-DD + ID, death domain and internal domain of IRAK4; MyD88-DD, death domain of MyD88; MyD88-DD + ID, death domain and internal domain of MyD88; MyD88-TIR, TIR domain of MyD88; Mal-TIR, TIR domain of Mal; TRAF, TNF receptor associated factor.

* Corresponding author. Tel.: +81 58 230 6386; fax: +81 58 230 6387.
** Corresponding author. Tel.: +81 75 383 2536; fax: +81 75 383 2541.
E-mail addresses: tochio@moleng.kyoto-u.ac.jp (H. Tochio), ohnishih@gifu-u.ac.jp (H. Ohnishi).
[1] Contributed equally as first authors.

0161-5890/$ – see front matter © 2013 Elsevier Ltd. All rights reserved.
http://dx.doi.org/10.1016/j.molimm.2013.11.008

formation can induce activation of the downstream signaling pathway, which eventually leads to the activation of NF-κB and activator protein 1 (AP-1).

Most previously identified causative mutations of human IRAK4 deficiency are nonsense or frame shift mutations that create early stop codons (Cardenes et al., 2006; Davidson et al., 2006; Enders et al., 2004; Krause et al., 2009; Ku et al., 2007; Medvedev et al., 2003; Picard et al., 2010; Takada et al., 2006; Yoshikawa et al., 2010), however, three missense mutations (M1V, R12C, and G298D) have been reported (Bouma et al., 2009; de Beaucoudrey et al., 2008; Hoarau et al., 2007). In human MyD88 deficiency, one nonsense mutation (E53X) and three missense mutations (E52del, L93P, and R196C) were reported as causative mutations (Conway et al., 2010; von Bernuth et al., 2008). Recently, new gene variations of *IRAK4* and *MyD88* have been deposited in the single nucleotide polymorphism (SNP) database following next-generation DNA sequencing, but the significance of these variants has not been evaluated. It is therefore important to establish methods to determine the association of gene variations with human diseases. For example, about MyD88, previous attempts have used western blotting, reporter gene assays, immunoprecipitation, and size exclusion chromatography of recombinant proteins to show that the SNPs MyD88 S34Y and R98C were loss-of-function variants (George et al., 2011), while another study used immunofluorescence to determine that S34Y fails to interact with IRAK4 (Nagpal et al., 2011).

Methods to detect the impaired responses to the Toll/interleukin-1 receptor agonists, such as enzyme-linked immunosorbent assay (ELISA) and flow-cytometry, are useful for rapid screening of innate immune deficiency syndromes (Davidson et al., 2006; Ohnishi et al., 2012a; Takada et al., 2006; von Bernuth et al., 2006). However, no *in vitro* method to assess the pathogenicity of novel variants of human *IRAK4*, *MyD88* and the other possible signaling components has been established. Therefore, when novel gene variants are found in that possible cases of IRAK4 or MyD88 deficiency syndromes, it is difficult to analyze the pathogenetic significance of these variants. In this study, we used a cell-based assay as well as *in vitro* protein-interaction analyses to show that IRAK4 R12C and R20W caused a loss of interaction with MyD88. This suggested that not only the loss of full-length IRAK4 and MyD88 protein expression but also the loss of Myddosome formation could cause IRAK4 and MyD88 deficiency syndromes.

2. Materials and methods

2.1. Cell culture

Human embryonic kidney (HEK) 293T cells were cultured in high glucose-containing DMEM (Invitrogen, Carlsbad, CA) supplemented with 10% heat-inactivated FBS (Sigma–Aldrich, St. Louis, MO), penicillin (100 U/ml), and streptomycin (100 μg/ml). Cells were incubated at 37 °C in a humidified atmosphere of 5% CO_2.

2.2. Vector preparations

cDNA encoding full-length IRAK4 (amino acid residues 1–460) or the DD and the internal domain (ID) of IRAK4 (IRAK4-DD + ID, amino acid residues 1–150) were tagged at the N terminus with a FLAG-epitope and cloned into the plasmid vector pcDNA3.1+ (Invitrogen). M1V was tagged at the C terminus because of a substitution of the start codon, and wild type (WT) tagged at the C terminus was prepared as a reference. Similarly, cDNA encoding full-length MyD88 (amino acid residues 1–296) or the TIR domain of MyD88 (MyD88-TIR, amino acid residues 148–296) tagged at the N terminus with a myc-epitope were cloned into the plasmid vector pcDNA3.1+ (Nada et al., 2012; Ohnishi et al., 2009). IRAK4 mutants and SNPs taken from dbSNP135 of the National Center for Biotechnology Information (NCBI, http://www.ncbi.nlm.nih.gov/snp) were generated using the GeneEditor *in vitro* Site-Directed Mutagenesis System (Promega, Fitchburg, WI). The pUNO hIL1R1(mb) vector (InvivoGen, San Diego, CA) was purchased and cDNA encoding IL-1RAcP and IL-18RAcPL were cloned into the plasmid vector pcDNA3.1+. The pGL4.32[luc2P/NF-κB-RE/Hygro] vector, used as an NF-κB luciferase reporter vector, and the pGL4.70[hRluc] vector, used as an internal control Renilla luciferase reporter vector, were purchased from Promega.

2.3. Western blot analysis

To detect protein expression, HEK293T cells were seeded on six-well plates at a density of 2×10^5/ml and transfected with 1 μg of expression plasmids of FLAG-tagged IRAK4 full length, FLAG-tagged IRAK4-DD, and myc-tagged MyD88 full length using Lipofectamine 2000 (Invitrogen) according to the manufacturer's instructions. After 48 h incubation, cells were harvested, washed with PBS, and lysed using CytoBuster Protein Extraction Reagent (Novagen, Darmstadt, Germany) containing a protease inhibitor mix (Roche Applied Science, Indianapolis, IN). All extracts were adjusted to contain equal amounts of total cellular proteins, as determined using the Bradford method. Supernatants and whole cell lysates were separated by electrophoresis on SDS polyacrylamide gels and transferred to nitrocellulose membranes using an iBlot Gel Transfer Device (Invitrogen). Membranes were blocked for 1 h in 5% BSA in TBST (pH 8.0, 10 mM Tris buffer containing 0.15 M NaCl and 0.1% Tween 20), then incubated at room temperature for 2 h with an anti-FLAG M2 monoclonal antibody (Sigma–Aldrich), anti-myc antibody (Invitrogen), or anti-β-actin antibody (Sigma–Aldrich) followed by incubation with anti-mouse IgG HRP conjugate (Promega) at room temperature for 30 min. Detection was performed using the ECL Chemiluminescent Substrate Reagent Kit (Invitrogen) and LightCapture system AE6970CP (ATTO, Tokyo, Japan).

2.4. NF-κB reporter gene activity

For the functional assessment of IRAK4, HEK293T cells, HEK293-hTLR1/2 cells (InvivoGen), HEK293-hTLR4-MD2-CD14 cells (InvivoGen) and HEK293-hTLR5 cells (InvivoGen) were transfected with NF-κB luciferase reporter vector, Renilla luciferase reporter vector, pcDNA3.1+ empty vector or pcDNA3.1+ FLAG-IRAK4 WT using Lipofectamine 2000. After transfection, cells were incubated for 24 h then stimulated with recombinant IL-1β (10 ng/ml) prepared as previously described (Wang et al., 2010), Pam3CSK4 (10 ng/ml, InvivoGen), LPS (10 ng/ml, Sigma–Aldrich), and recFLA-ST (10 ng/ml, InvivoGen) for 6 h. In a similar way, HEK293T cells were transfected as described above and with IL-18RAcPL, and stimulated with recombinant IL-18 (50 ng/ml) prepared as previously described (Kato et al., 2003; Li et al., 2003) for 6 h. Luciferase reporter gene activities were analyzed using the Dual-Luciferase Reporter Assay System (Promega). Similarly, HEK293T cells were transfected with pUNO-hIL1R1 vector, pcDNA3.1+ IL-1RAcP vector, NF-κB luciferase reporter vector, Renilla luciferase reporter vector, pcDNA3.1+ empty vector or pcDNA3.1+ FLAG-IRAK4 WT or variants, as described above. After transfection, cells were incubated for 24 h and luciferase reporter gene activities were analyzed.

For the functional assessment of MyD88, HEK293T cells were transfected with NF-κB luciferase reporter vector, Renilla luciferase reporter vector, and different amounts of pcDNA3.1+ myc-MyD88

WT or variants (5, 15 or 50 ng). The amounts of transfected plasmid were adjusted to an equal amount with pcDNA3.1+ empty vector. After transfection, cells were incubated for 24 h. To compare the dominant negative effect of MyD88, pcDNA3.1+ myc-MyD88-TIR WT or variants (5, 15 or 50 ng), pcDNA3.1+ IL-18RAcPL, NF-κB luciferase reporter vector, and Renilla luciferase reporter vector were co-transfected, and then, cells were incubated for 24 h and stimulated with/without IL-18 (10 ng/ml) for 6 h. Luciferase reporter gene activities were analyzed as described above.

The NF-κB activation of each condition was assessed in at least three independent experiments. The statistical significance of the differences in luciferase activities was determined using one-way ANOVA with Bonferroni's post-hoc test. The statistical significance was defined as $P < 0.05$.

2.5. Protein preparation

The portion of the human *IRAK4* gene encoding the DD + ID (amino acid residues 1–150) and the human *MyD88* gene encoding the DD and the ID (MyD88-DD + ID, amino acid residues 1–152) were cloned into vector pGEX-6P-1 (GE Healthcare, Little Chalfont, UK). These vectors were transformed into *Escherichia coli* BL-21 (DE3) (Novagen). IRAK4-DD + ID variants and MyD88-DD + ID, which were expressed as GST fusion proteins, were first purified by glutathione Sepharose 4B FF (GE Healthcare) affinity chromatography, and the GST-tag was removed by digestion with PreScission protease (GE Healthcare). Subsequently, the DD + IDs were purified by anion exchange chromatography (Q-Sepharose column; GE Healthcare) and gel filtration (Superdex 75 HR 26/60 column; GE Healthcare). Using a similar purification protocol, ^{1}H–^{15}N-labeled MyD88-DD + ID was prepared. All nuclear magnetic resonance (NMR) samples were uniformly ^{15}N-labeled and prepared in 210 μl solutions of H_2O/D_2O (95%/5%) containing 20 mM potassium phosphate buffer at pH 6.0 with 10 mM DTT. The portions of the human TIR domains of MyD88 WT and its mutants (M178I, R196C) and MyD88 adaptor-like (Mal) (Mal-TIR, amino acid residues 75–235) were cloned into pGEX-5X-1 and pGEX5X-3 vectors (GE Healthcare), respectively. The proteins were purified as previously described (Ohnishi et al., 2009).

2.6. Analytical gel filtration

Molecular masses of the purified recombinant proteins IRAK4-DD + ID and MyD88-DD + ID were evaluated by size exclusion chromatography. Gel filtration analysis was performed using a Superdex-200 10/300 GL column (GE Healthcare) attached to an AKTA purifier (GE Healthcare) at 10 °C. The column was equilibrated with 20 mM HEPES buffer (pH 7.0), 100 mM KCl, 10 mM DTT and 1 mM EDTA. The column was calibrated using a gel filtration standard kit (Bio-Rad, Hercules, CA). A total of 100 μl of 100 μM IRAK4-DD + ID and 100 μM MyD88-DD + ID proteins was applied to the gel filtration column. Protein elution was monitored by UV absorption at 280 nm. The molecular masses of these proteins were estimated using a calibration curve.

2.7. GST pull-down assays

GST-fusion proteins of MyD88-TIR and purified proteins of the TIR domain of Mal were incubated with Glutathione Sepharose 4B (GE Healthcare) in binding buffers (20 mM potassium phosphate buffer (pH 6.0), 0.1 mM EDTA, 10 mM DTT, and 0.2% Triton X-100) for 16 h. After four wash steps using 20 mM potassium phosphate buffer (pH 6.0), 100 mM KCl, 0.1 mM EDTA, 10 mM DTT, and 0.2% Triton X-100, the resin was analyzed by SDS-PAGE and Coomassie Brilliant Blue staining.

2.8. NMR titration

An aliquot of 0.25 equivalent amounts of non-labeled IRAK4 WT or its variants was added to 210 μl of 50 μM ^{15}N-labeled MyD88-DD + ID, with the exception for R20W, up to its 2.0 equivalent amounts. For the titration with R20W IRAK4-DD + ID, 25 μM MyD88-DD + ID was used. The samples were in 20 mM potassium phosphate (pH 6.0) and 10 mM DTT in H2O/D2O (95%/5%). At each titration point, 2D ^{1}H–^{15}N SOFAST-HMQC spectra were recorded at 298 K on Bruker Avance II 700 MHz spectrometer equipped with cryogenic probes. The 2D spectra were processed using NMRPipe (Delaglio et al., 1995) and analyzed using the Sparky (Goddard and Kneller, 1999) analysis software, whereas 1D projections were generated using Bruker TopSpin 3.1. A well-resolved NMR signal derived from a Trp sidechain aromatic ^{1}H–^{15}N pair in the projection was selected (supplementary Fig. S1B) at each titration point, and then intensities were normalized with the intensity of the corresponding NMR signal of ^{15}N MyD88-DD + ID recorded in the absence of IRAK4-DD + ID (Ohnishi et al., 2009). The normalized intensities were plotted as a function of the equivalent molar amounts of the titrant.

2.9. Protein stability assay

HEK293T cells were seeded on six-well plates at a density of 2×10^5/ml and transfected with 1 μg of expression plasmids Flag-tagged IRAK4-DD using Lipofectamine 2000. After 48 h, cells were treated with 25 μM cycloheximide for 0, 24, 48, and 72 h (Fukao et al., 1999). Cellular extracts were prepared in CytoBuster Protein Extraction Reagent containing complete protease inhibitor mix. All extracts were adjusted to contain equal amounts of total cellular proteins, as determined using the Bradford method. Western blot analysis with anti-FLAG antibody was carried out using standard protocols as described above.

3. Results

3.1. Cell-based assays of IRAK4 variants

3.1.1. Protein expression of IRAK4

To functionally characterize the genetic variants of *IRAK4*, FLAG-tagged full-length expression constructs corresponding to the loss-of-function mutations that were previously reported as pathogenic mutations ('*IRAK4* mutants') and nonsynonymous SNPs ('*IRAK4* SNPs') were generated. In this study, we selected the six IRAK4 mutants (M1V, a missense mutation of start codon reported in Slovenia (de Beaucoudrey et al., 2008); R12C, a missense mutation reported in France and located in the DD (Hoarau et al., 2007); c.118insA and R183X, mutations reported in Japan that include a frame shift mutation (Picard et al., 2010; Takada et al., 2006); Q293X, the most common mutation in Europe (Picard et al., 2010); G298D, a missense mutation reported in UK and located in the kinase domain (Bouma et al., 2009)) and five SNPs in the DD (Fig. 1A). Our five SNPs were all within the DD as we focused on the interaction between IRAK4 and MyD88.

No protein expression could be detected of the three *IRAK4* mutations M1V, Q293X, and c.118insA. R183X expressed a smaller protein than WT, while G298D protein expression levels were decreased (Fig. 1B). The expression of R12C was comparable with WT as were expression levels of all SNPs (Fig. 1C).

3.1.2. Inhibition of NF-κB activation of IRAK4

Next, *IRAK4* variants were tested for NF-κB reporter gene activity using a dual luciferase assay system. As Medvedev et al.

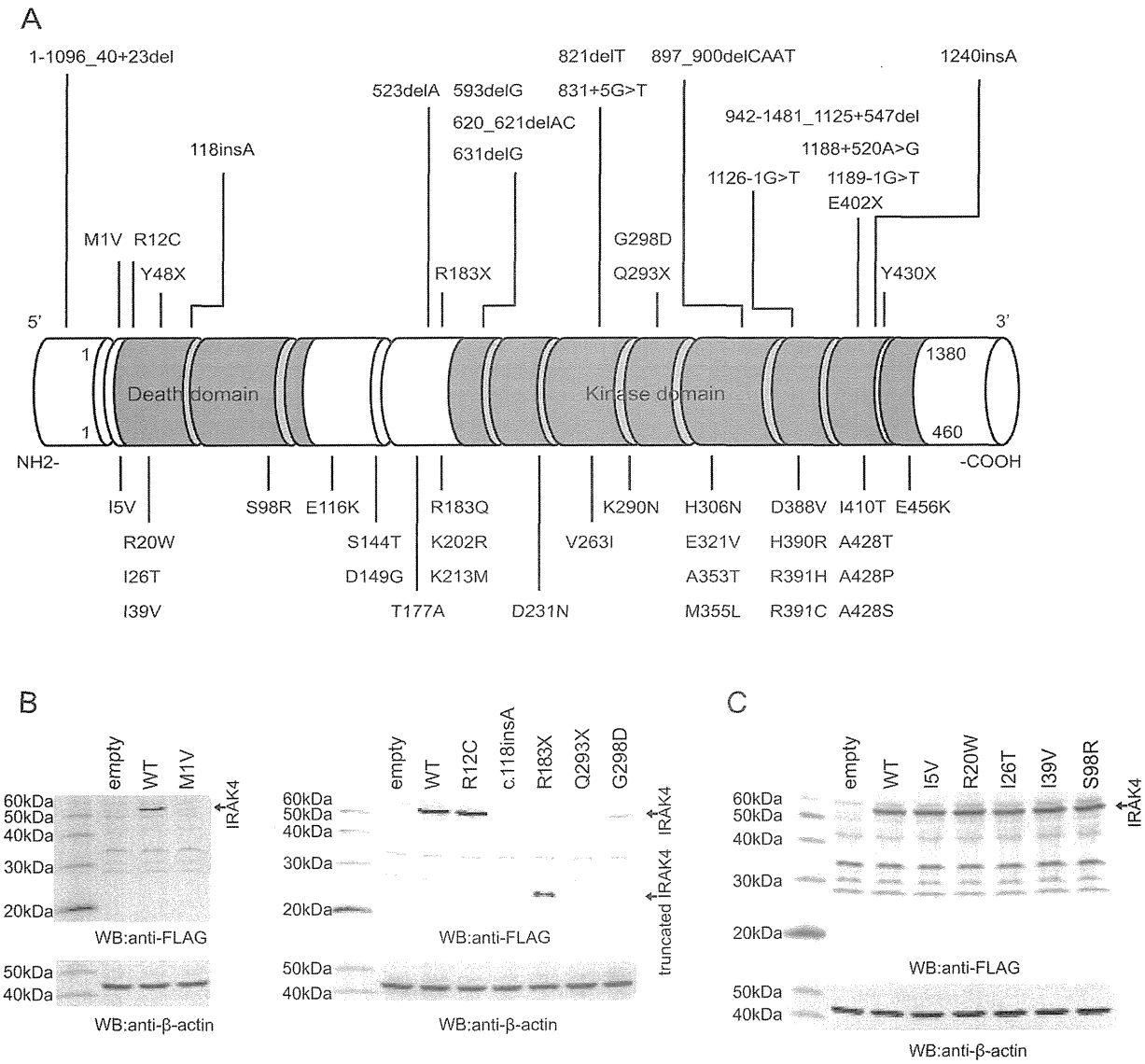

Fig. 1. Protein expression of *IRAK4* variants. (A) Schematic representation of *IRAK4* showing all identified mutations and nonsynonymous SNPs. *IRAK4* consists of 12 exons and the protein is composed of an N-terminal death domain and C-terminal kinase domain. Mutations are annotated at the upper side of this schema, and SNPs at the lower. (B) Expression levels of *IRAK4* mutants in HEK293T cells. Protein expression of M1V, Q293X, and c.118insA could not be detected. R183X expressed a truncated protein and the expression level of G298D was low. (C) Expression levels of *IRAK4* SNPs in HEK293T cells. All SNPs examined in this study expressed protein at the same level as WT.

(2003) previously reported that IL-1β-induced NF-κB activation was inhibited by overexpressed IRAK4 in HEK293T cells, we repeated their method with five different HEK293 cell lines and their appropriate ligands to compare the inhibition of NF-κB activation (Fig. 2). IL-1β, IL-18 and the ligands of TLR1/2, TLR4, and TLR5-induced NF-κB activations were not significantly inhibited by overexpressed IRAK4 (Fig. 2A–E), but the NF-κB activity enhanced by both transiently transfected IL-1R1 and IL-1RAcP could be significantly inhibited by overexpressed IRAK4 (Fig. 2F).

This system was used to compare *IRAK4* variants. Fig. 2G shows that NF-κB activation of the mutants c.118insA, R183X, Q293X, and G298D was less inhibited than WT. However, R12C showed a similar activity level to WT, although this mutation was previously reported to be a loss-of-function mutant in a human IRAK4 deficiency patient (Hoarau et al., 2007). Fig. 2H shows that all *IRAK4* SNPs significantly inhibited NF-κB activity to the same extent as WT. Only R20W showed a stronger inhibitory effect.

3.2. Cell-based assays of MyD88 variants

3.2.1. Protein expression of MyD88

We analyzed four previously reported loss-of-function mutations of MyD88: E52del, E53X, and L93P located in the DD, and R196C located in the TIR domain, as well as three SNPs: S34Y and R98C (loss-of-function variants (George et al., 2011; Nagpal et al., 2011) located in the DD, and M178I in the TIR domain (Fig. 3A). To functionally characterize the *MyD88* genetic variants, myc-tagged full-length expression constructs corresponding to the loss-of-function mutations ('*MyD88* mutants') and nonsynonymous SNPs ('*MyD88* SNPs') were generated. No protein expression was detected of S34Y and E53X, while expression of E52del and L93P was very low. On the other hand, expression levels of R98C, M178I, and R196C were similar to WT (Fig. 3B).

3.2.2. NF-κB activity of MyD88

Next, we assessed the abilities of *MyD88* variants to activate the NF-κB signaling pathway using a dual luciferase assay system in

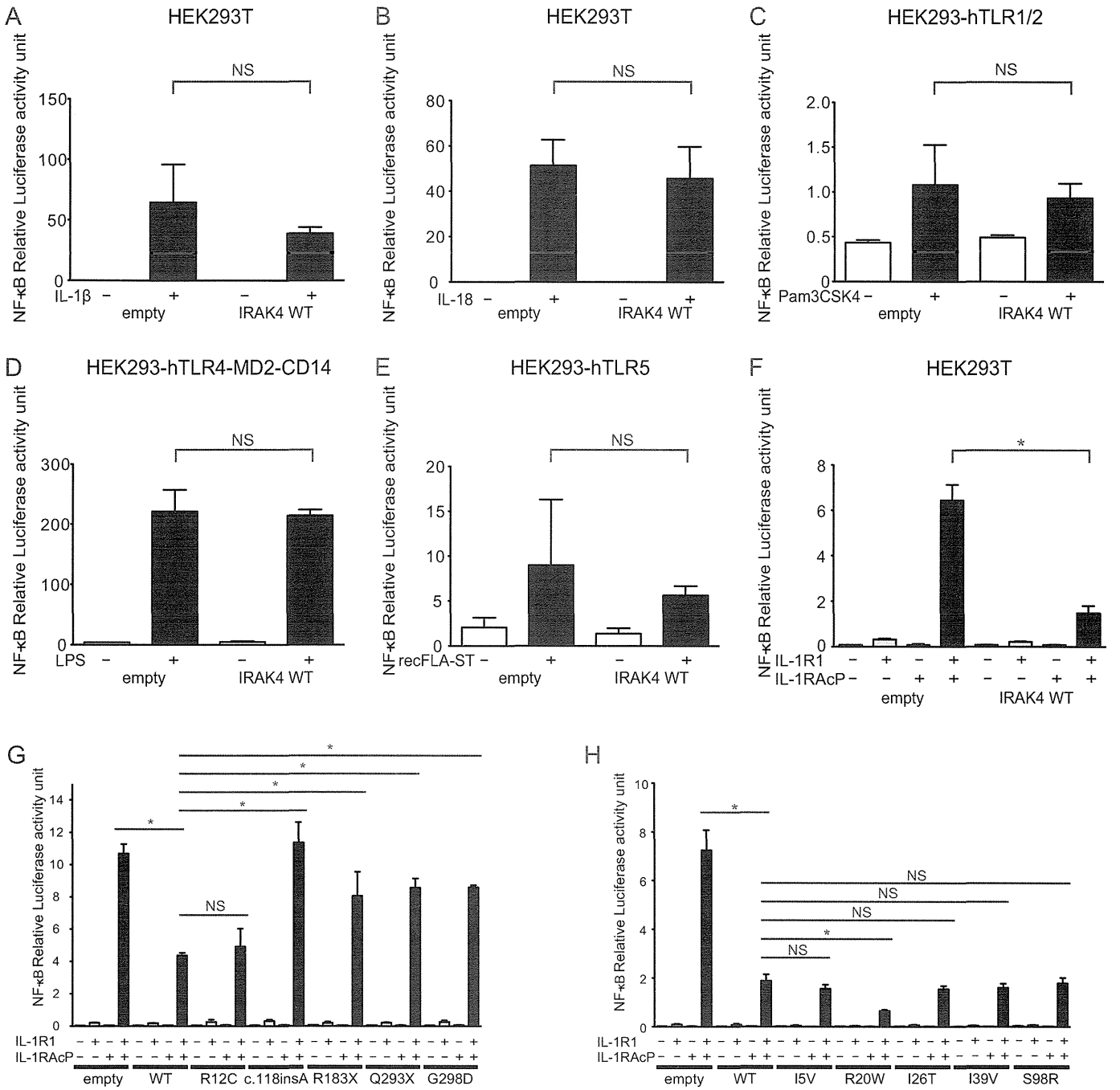

Fig. 2. Cell-based NF-κB activity assays of *IRAK4* variants. (A-F) The inhibition of NF-κB activation in five different cell lines by IRAK4. IL-1β- (10 ng/ml), IL-18- (50 ng/ml), Pam3CSK4- (10 ng/ml), LPS- (10 ng/ml) and recFLA-ST- (10 ng/ml) induced NF-κB activations was not significantly inhibited by overexpressed IRAK4 WT in HEK293T cells (A, B, F), HEK293-hTLR1/2 cells (C), HEK293-hTLR4-MD2-CD14 cells (D), and HEK293-hTLR5 cells (E). Transient transfection of both IL-1R1 and IL-1RAcP significantly enhanced NF-κB activity in HEK293T cells, which could be significantly inhibited by overexpressed IRAK4. (G and H) The inhibition of NF-κB activation by *IRAK4* variants in HEK293T cells. The inhibition by mutants c.118insA, R183X, Q293X, and G298D of NF-κB activation induced by co-transfection both IL-1R1 and IL-1RAcP was significantly less than in WT. R12C showed a similar inhibition level to WT. All *IRAK4* SNPs significantly inhibited NF-κB activity as well as WT. Only R20W showed a stronger inhibition of NF-κB activity than WT. Data represent the mean ± SD of a representative experiment ($n = 3$). Asterisk indicates a statistically significant difference between WT and the others. NS means "not-significant".

HEK293T cells. Fig. 3C shows that overexpression of S34Y, E52del, E53X, L93P, R98C, and R196C resulted in lower NF-κB activation than that of WT. We previously reported that the truncated MyD88 lacking a DD (MyD88-TIR) inhibited IL-18-stimulated NF-κB activation by means of a dominant negative effect (Ohnishi et al., 2012b). Therefore, in the present study, we examined NF-κB activation inhibition from a dominant-negative effect in HEK293T cells transiently co-transfected with IL-18RAcP and MyD88-TIR WT, or M178I and R196C (Fig. 3D). MyD88-TIR M178I inhibited NF-κB activation to a similar level as WT, but MyD88-TIR R196C was compromised in its effect to inhibit NF-κB activation.

3.3. GST pull-down assay of MyD88-TIR to Mal-TIR

MyD88 interacts with Mal via a shared TIR domain and activates a downstream signaling pathway. To analyze the mutations